frontiers

Supplementary Material

1 Supplementary Figures and Tables

Table S1. Origin and composition of compound classes derived from CuO products

CuO product	Sub-products	Origin	Additional information
Vanillyl phenols (VP)	Vanillin (Vl), Acetovanillone (Vn), Vanillic acid (Vd)	Terrestrial[1]	Angiosperm and gymnosperm plants[1]
Syringyl phenols (SP)	Syringealdehyde (Sl), Acetosyringone (Sn), Syringic acid (Sd)	Terrestrial[1]	Angiosperm plants[1]
Cinnamyl phenols (CP)	p-Coumaric acid (pCd), Ferulic acid (Fd)	Terrestrial[1]	Non-woody vascular plant tissues (i.e. leaves, needles, grasses)[1]
Cutin acids (CA)	16-Hydroxyhexadecanoic acid (w-C_{16}), Hexadecan-1,16-dioic acid (C_{16}DA), 8 or 9 or 10,16-Dihydroxy C_{16} acids(x,w-C_{16}), 7 or 8-Dihydroxy C_{16} α,ω-dioic acid (x-C_{16}DA)	Terrestrial	Non-woody tissues (i.e. leaves, needles, grasses)[2]
p-hydroxybenzenes (PB)	p-Hydroxyacetophenone (Pn), p-Hydroxybenzaldehyde (Pl), p-Hydroxybenzoic acid (Pd)	Heterogenous	Terrestrial: woody and herbaceous tissues[3,4] Marine: phytoplankton and bacterial biomass[3,4]
Benzoic acids (BA)	Benzoic acid (Bd), m-Hydroxybenzoic acid (mBd), 3,5-Dihydroxybenzoic acid (3,5-Bd)	Heterogenous	Terrestrial: humification processes in soil[3,4] Marine: phytoplankton biomass[3,4]
Amino acids (AA)	Butan-1,4-dioic acid (C_4DA), 2-Buten-1,4-dioic acid (C_4DA:1), 2-Carboxypyrrole acid (Cp), Phenylglyoxylic acid (Pg)	Heterogenous	Terrestrial: proteic material (i.e. bacteria, fungi)[3] Marine: proteic material (i.e. zooplankton, phytoplankton)[3]
Di-carboxylic acids (DA)	Penten-1,5-dioic acid (C_5DA), Hexan-1,6-dioic acid (C_6DA), Heptan-1,7-dioic acid (C_7DA), Octan-1,8-dioic acid (C_8DA), Nonan-1,9-dioic acid (C_9DA), Decan-1,10-dioic acid (C_{10}DA), Undecan-1,11-dioic acid (C_{11}DA), Dodecan-1,12-dioic acid (C_{12}DA)	Heterogenous	Terrestrial: multiple sources, abundant in soil, bacteria[3] Marine: multiple sources, abundant in phytoplankton[3]
Fatty acids (FA)	Decanoic acid (C_{10}FA), Dodecanoic acid (C_{12}FA), Tetradecanoic acid (C_{14}FA), Hexadecenoic acid (C_{16}FA:1), Hexadecanoic acid (C_{16}FA), Octadecenoic acid (C_{18}FA:1), Octadecanoic acid (C_{18}FA)	Heterogenous	Terrestrial: lipidic material (i.e. bacteria, fungi)[3] Marine: lipidic material (i.e. zooplankton, phytoplankton)[3]

[1]Hedges and Mann, 1979; [2]Goñi and Hedges, 1990; [3]Goñi and Hedges, 1995; [4]Prahl et al., 1994

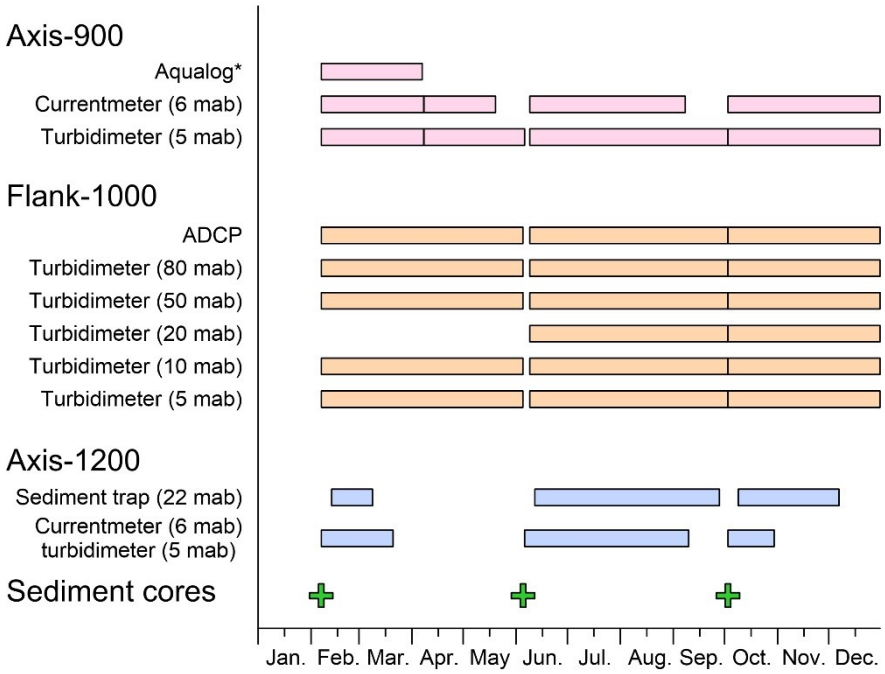

Figure S1. Time diagram of the available time series from the instruments installed in the Axis-900, in the Flank-1000 and in the Axis-1200 moorings. *Data of the Aqualog and the corresponding current meter and turbidimeter of that time-frame are presented in detail in Arjona-Camas et al., 2021.

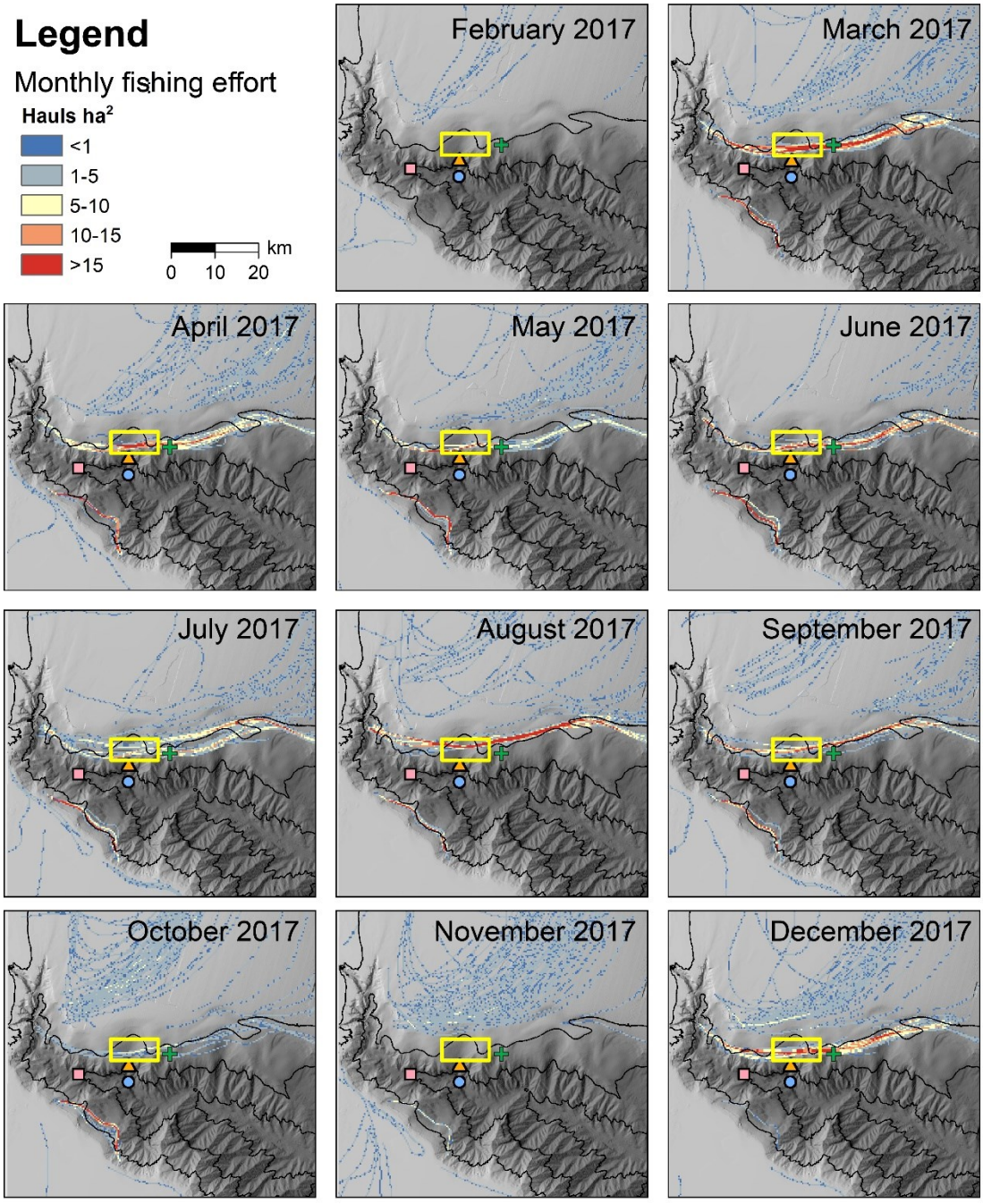

Figure S2. Monthly fishing effort (hauls per hectare) in Palamós Canyon from February to December 2017.

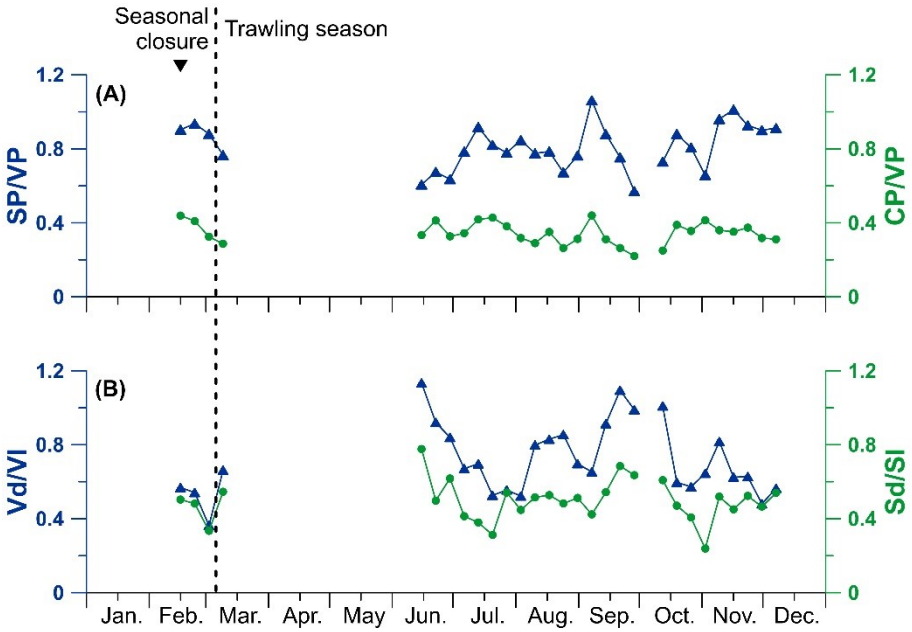

Figure S3. Temporal evolution of terrigenous biomarker signatures. **a)** syringyl to vanillyl ratios (SP/VP) and cinnamyl to vanillyl ratios (CP/VP). **b)** acid to aldehyde ratios of vanillic acid to vanillin (Vd/Vl) and syringic acid to syringealdehyde (Sd/Sl).

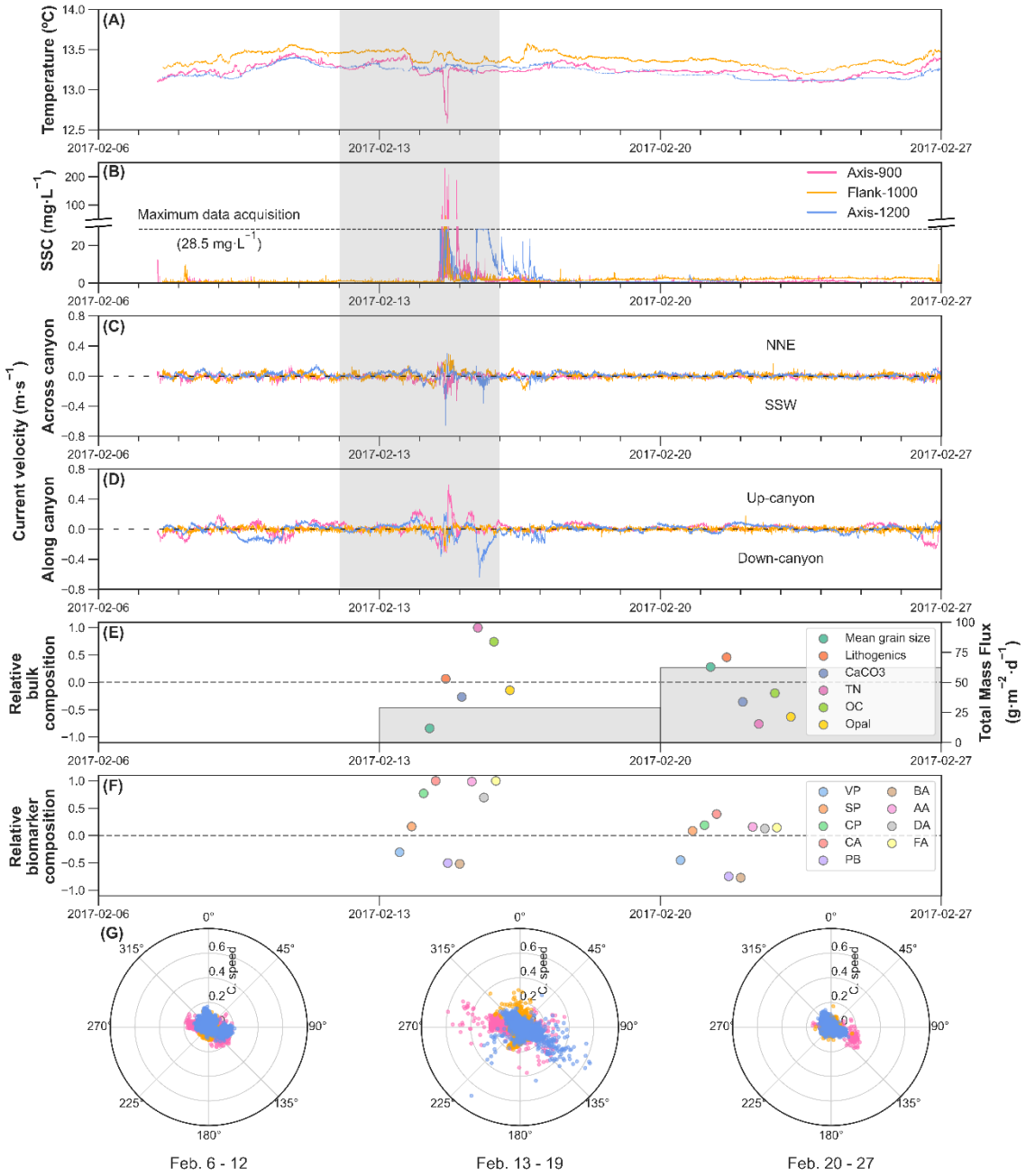

Figure S4. Time-series during the eastern storm in February: **(A)** temperature, **(B)** suspended sediment concentration (SSC), **(C)** across-canyon current velocity, and **(D)** along-canyon current velocity of Axis-900, Axis-1200, and Flank-1000 moorings at 5 mab (Axis-900 and Axis-1200) and 10 mab (Flank-1000). Weekly values of **(E)** total mass flux and relative variations of bulk composition, **(F)** relative variations in the biomarker compound classes, and **(G)** polar plots of current direction and current speed (radius) at 5 mab (Axis-900 and Axis-1200) and 10 mab (Flank-1000). The relative contribution of the sediment trap composition (**(E)** and **(F)**) are weekly averages, and their position along the x-axis are just to simplify the graphical visualization. Note the maximum data acquisition of SSC for Axis-1200 (28.5 mg·L^{-1}). The extension of the February eastern storm and dense shelf water cascading event is marked by a grey rectangle in **(A)** to **(D)**, and not in **(E)** to **(G)** since these subplots represent weekly average values.

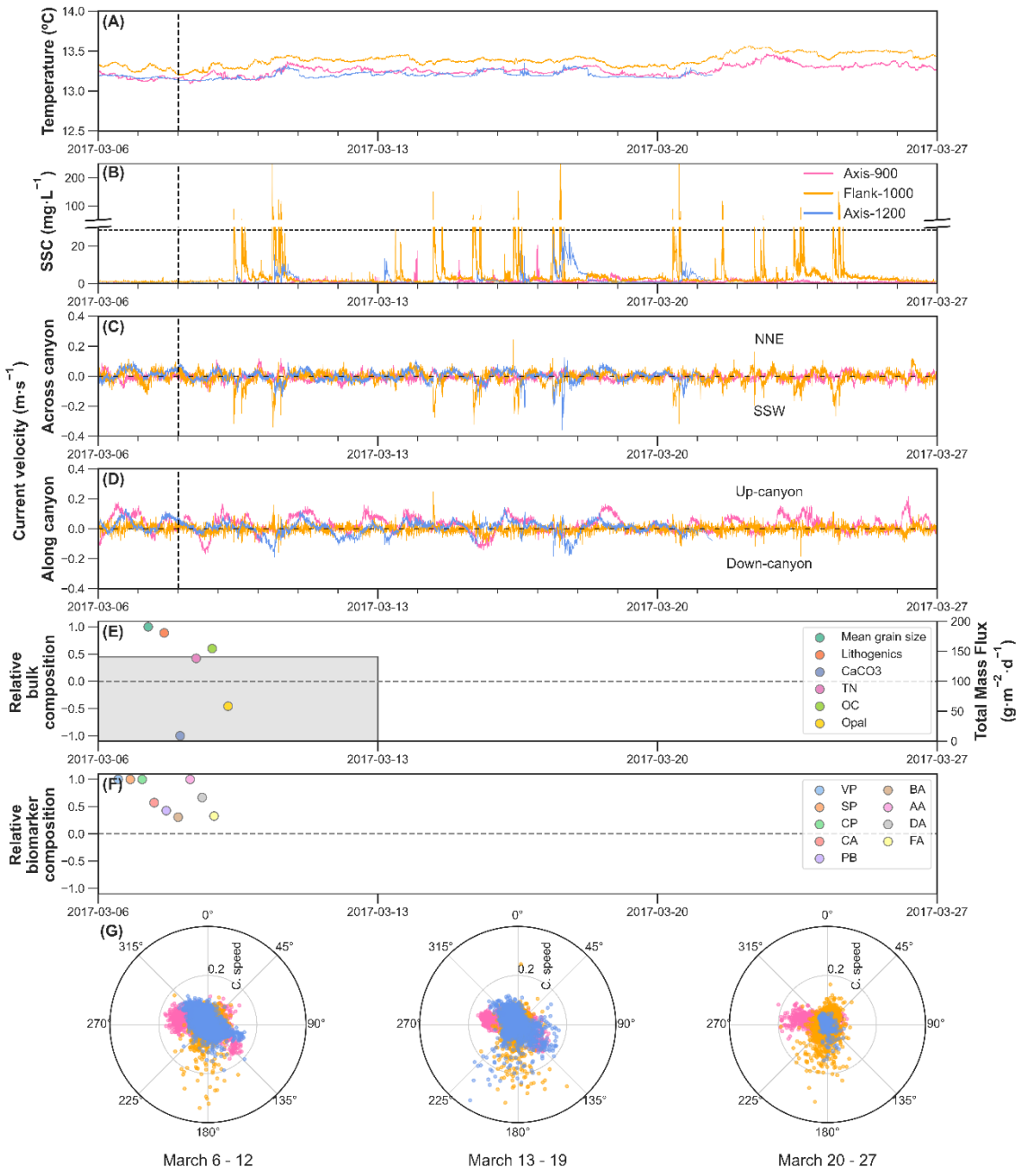

Figure S5. Time-series during the beginning of the trawling season: **(A)** temperature, **(B)** suspended sediment concentration (SSC), **(C)** across-canyon current velocity, and **(D)** along-canyon current velocity of Axis-900, Axis-1200, and Flank-1000 moorings at 5 mab (Axis-900 and Axis-1200) and 10 mab (Flank-900). Weekly values of **(E)** total mass flux and relative variations of bulk composition, **(F)** relative variations in the biomarker compound classes, and **(G)** polar plots of current direction and current speed (radius) at 5 mab (Axis-900 and Axis-1200) and 10 mab (Flank-1000). The relative contribution of the sediment trap composition (**(E)** and **(F)**) are weekly averages, and their position along the x-axis are just to simplify the graphical visualization. Note the maximum data acquisition of SSC for Axis-1200 (28.5 mg·L^{-1}) and that sensors recorded data until March 21 (Fig. S1). The vertical dashed line in **(A)** to **(D)** represents the onset of bottom trawling activity on March 8, which is not shown in **(E)** to **(G)** since these subplots represent weekly average values.

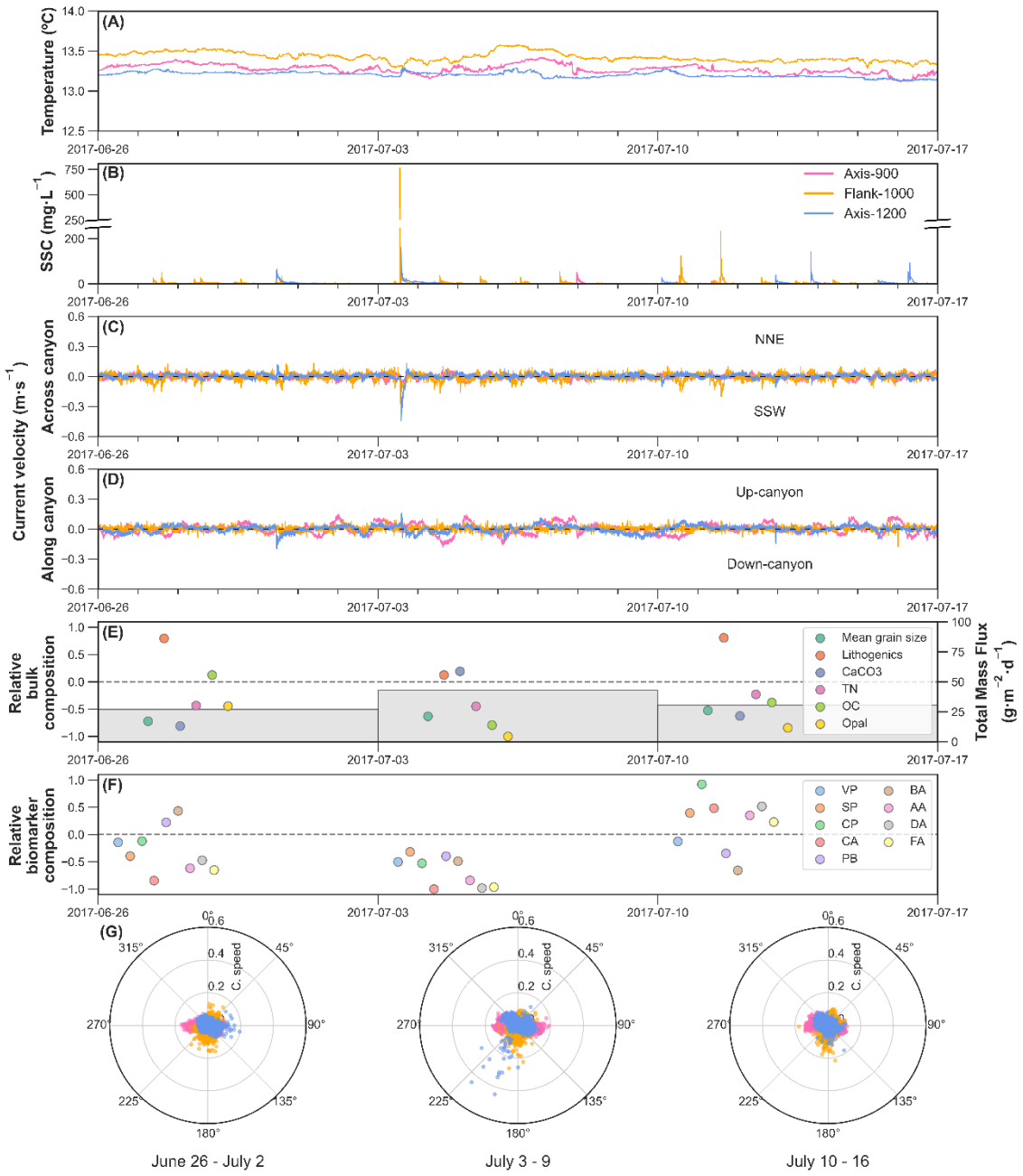

Figure S6. Time-series of three specific weeks during the trawling season: **(A)** temperature, **(B)** suspended sediment concentration (SSC), **(C)** across-canyon current velocity, and **(D)** along-canyon current velocity of Axis-900, Axis-1200, and Flank-1000 moorings at 5 mab (Axis-900 and Axis-1200) and 10 mab (Flank-1000). Weekly values of **(E)** total mass flux and relative variations of bulk composition, **(F)** relative variations in the biomarker compound classes, and **(G)** polar plots of current direction and current speed (radius) at 5 mab (Axis-900 and Axis-1200) and 10 mab (Flank-1000). The relative contribution of the sediment trap composition (**(E)** and **(F)**) are weekly averages, and their position along the x-axis are just to simplify the graphical visualization.

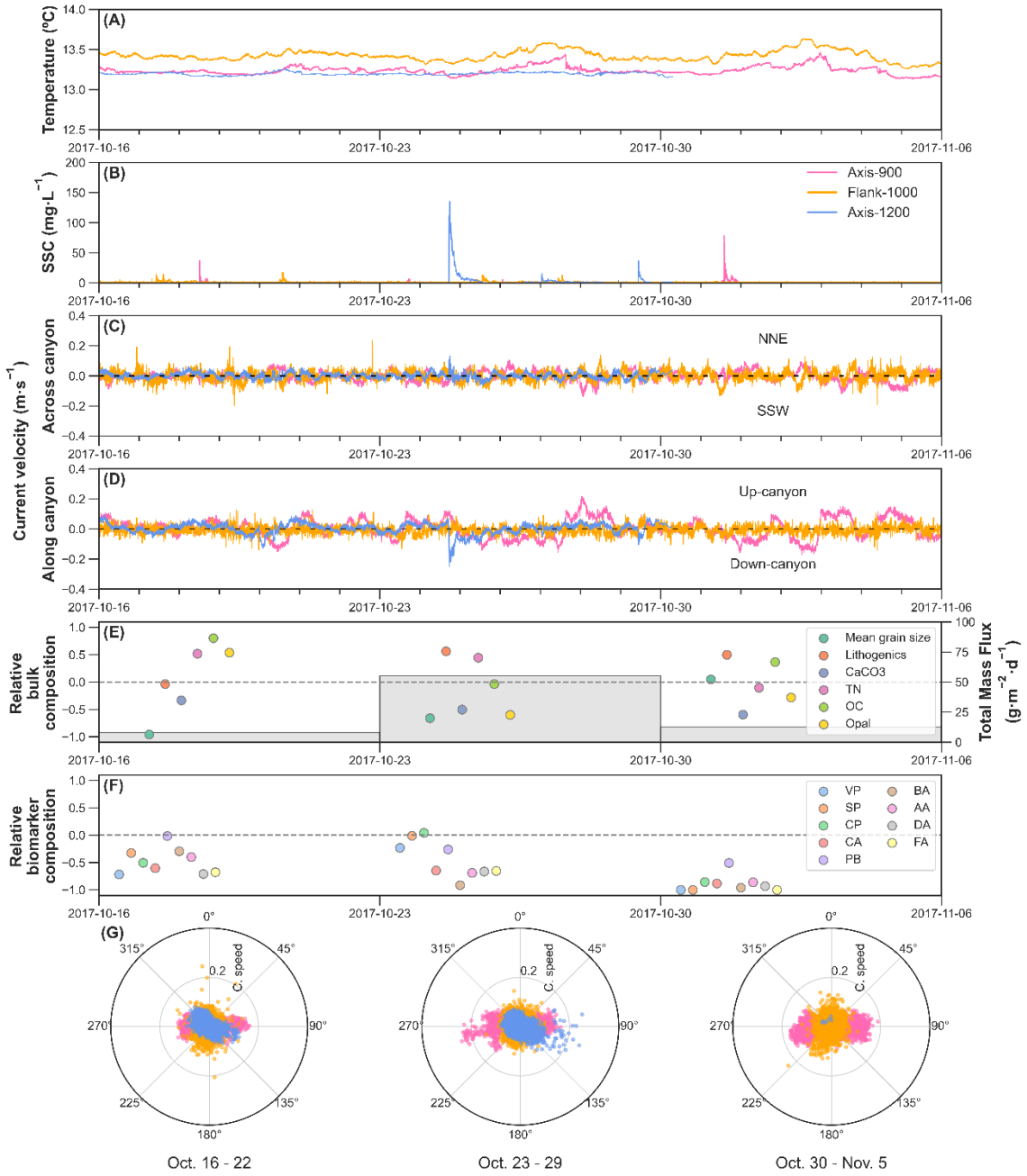

Figure S7. Time-series of the late-October sediment transport event during the intermission of bottom trawling in the adjacent flank: **(A)** temperature, **(B)** suspended sediment concentration (SSC), **(C)** across-canyon bottom current speed, and **(D)** along-canyon current velocity of Axis-900, Axis-1200 and Flank-1000 moorings at 5 mab (Axis-900) and 10 mab (Flank-1000). Weekly values of **(E)** total mass flux and relative variations of bulk composition, **(F)** relative variations in the biomarker compound classes, and **(G)** polar plots of current direction and current speed (radius) at 5 mab (Axis-900 and Axis-1200) and 10 mab (Flank-1000). The relative contribution of the sediment trap composition ((**E**) and (**F**)) are weekly averages, and their position along the x-axis are just to simplify the graphical visualization. Note that the sensors of Axis-1200 recorded data until October 30 (Fig. S1).

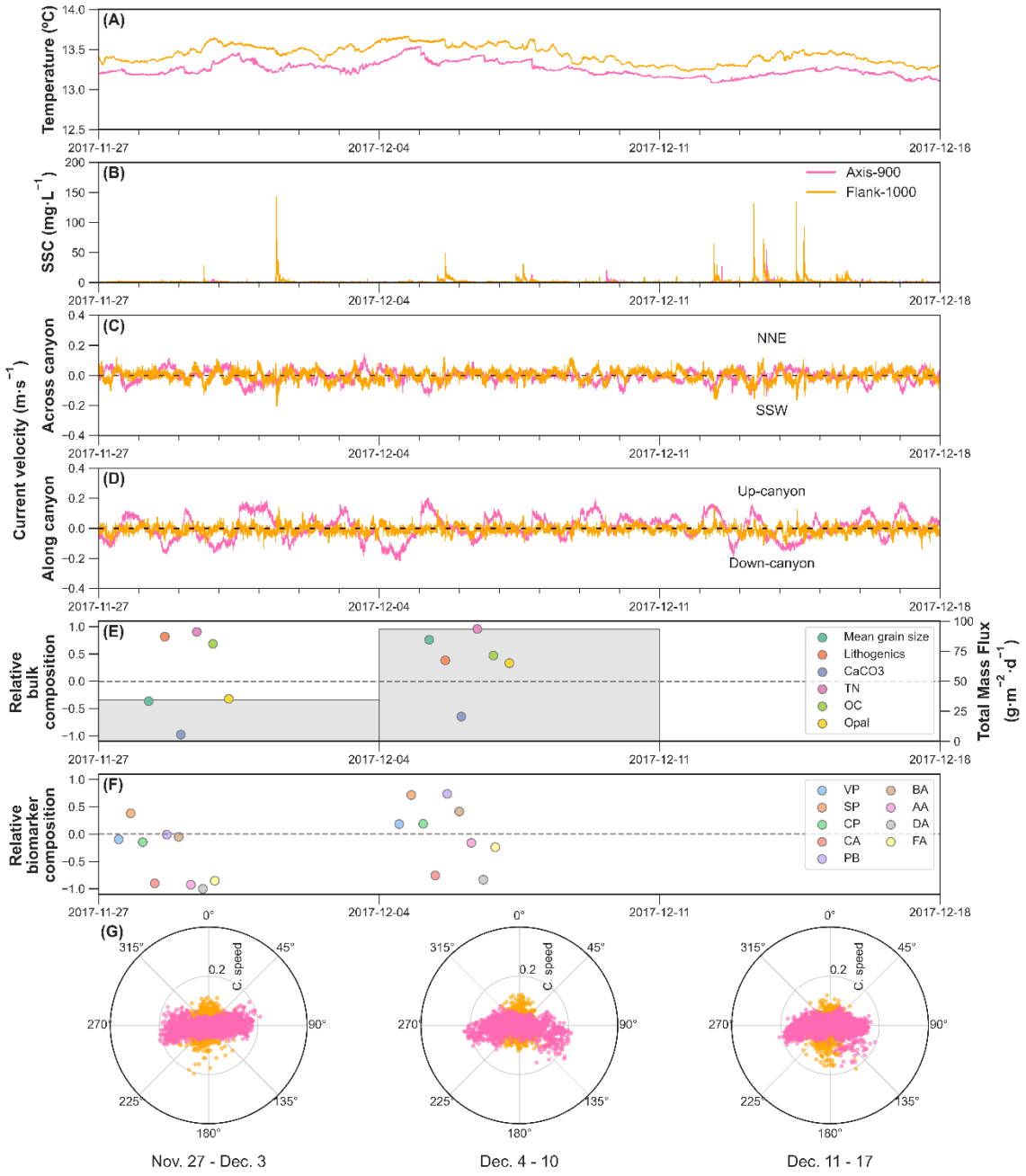

Figure S8. Time-series of the intermission of bottom trawling activities in November and its resume in early December: **(A)** temperature, **(B)** suspended sediment concentration (SSC), **(C)** across-canyon current velocity, and **(D)** along-canyon current velocity of Axis-900 and Flank-1000 moorings at 5 mab (Axis-900) and 10 mab (Flank-1000). Weekly values of **(E)** total mass flux and relative variations of bulk composition, **(F)** relative variations in the biomarker compound classes, and **(G)** polar plots of current direction and current speed (radius) at 5 mab (Axis-900) and 10 mab (Flank-1000). The relative contribution of the sediment trap composition (**(E)** and **(F)**) are weekly averages, and their position along the x-axis are just to simplify the graphical visualization. Note that the sensors of Axis-1200 mooring didn't work during this period (Fig. S1).